·Article·
Advances in Polar Science
doi: 10.3724/SP.J.1085.2013.00019
March 2013 Vol. 24 No. 1: 19-31

Statistical characteristics of ionospheric backscatter observed by SuperDARN Zhongshan radar in Antarctica

HU Hongqiao[1], LIU Erxiao[1,2*], LIU Ruiyuan[1], YANG Huigen[1] & ZHANG Beichen[1]

[1] SOA Key Laboratory for Polar Science, Polar Research Institute of China, Shanghai 200136, China;
[2] School of Science, Xidian University, Xi'an 710071, China

Received 10 December 2012; accepted 27 January 2013

Abstract Zhongshan HF radar, as one component of SuperDARN, has been established and in operation since April, 2010. Using data from the first two years of its operation, this paper investigates the radar's performance, the diurnal and seasonal variations of ionospheric echoes, and their dependence on geomagnetic activity. Statistical studies show that the occurrence of echoes in different beams varies at different frequencies, which arises from the direction of the beam and the area over which the beam can achieve the orthogonality condition between the wave vector and the Earth's magnetic field. The diurnal variation is obvious with double peak structures both in the occurrence rate and average power at 04–08 UT and 16–17 UT. The line-of-sight velocities are mainly positive on the dayside and negative on the nightside for Beam 0, which is the opposite of the trend for Beam 15. The spectral widths on the dayside are often higher than those on the nightside owing to the high energy particle precipitation in the cusp region. The seasonal variations are more obvious for those beams with larger numbers. The occurrence, the average power, the line-of-sight velocity, and the spectral widths are generally larger in the winter months than in the summer months. The influence of geomagnetic activity on radar echoes is significant. The peak echo occurrence appears on the dayside during geomagnetically quiet times, and shifts toward the nightside and exhibits an obvious decrease with increasing *K*p. With increasing geomagnetic activity, the line-of-sight velocities increase, whereas the spectral widths decrease. The frequency dependence is investigated and it is found that in the operating frequency bands in 2010, 9–10 MHz is the most appropriate band for the SuperDARN Zhongshan radar.

Keywords **SuperDARN, Zhongshan radar, diurnal variations, seasonal variations, geomagnetic activity dependence, frequency dependence**

Citation: Hu H Q, Liu E X, Liu R Y, et al. Statistical characteristics of ionospheric backscatter observed by SuperDARN Zhongshan radar in Antarctica. Adv Polar Sci, 2013, 24:19-31, doi: 10.3724/SP.J.1085.2013.00019

1 Introduction

High frequency (HF) coherent radar backscatter from ionospheric plasma irregularities with a variety of scale-lengths from meters to kilometers, also known as radar aurora, is an important high-latitude phenomenon. These irregularities are thought to drift with the bulk plasma motion and are believed to be generated by several kinds of instabilities. Consequently, much emphasis has been given to understanding why and where these ionospheric irregularities occur, and what the favorable conditions for their generation are. In the F region, the irregularities are generated primarily by the gradient drift instability[1-2] and the current-convective instability[3-4], whereas in the E region altitude, the bulk of the plasma irregularities are believed to be generated by two possible mechanisms: The modified two-stream instability, also known as the Farley-Buneman instability(FBI), and the gradient-drift instability (GDI)[5], producing two categories of echoes, termed Type I and Type II, respectively. Type I echoes have a low spectral width and a velocity constrained to be near the local ion-acoustic speed Cs with a typical value of 350–400 $m \cdot s^{-1}$ at 110 km altitude. Type II echoes have a lower Doppler velocity and a broader spectral width.

Greenwald et al.[6-7] developed the concept of the

* Corresponding author: Liu Erxiao (email: liuerxiao@pric.gov.cn)

Super Dual Auroral Radar Network (SuperDARN) capable of monitoring extensive regions of both the northern and southern hemisphere polar ionospheres; especially the auroral and polar cap ionospheres. The concept is based on the development of a network of dual radars. Each radar pair comprises two separate radars that have an overlapping field of view, such that the velocity of the irregularities can be determined owing to the different viewing directions of the radars. Currently, SuperDARN consists of more than 30 radars globally and the radar data are utilized by scientists from all over the world.

In developing the Zhongshan HF radar, the aim has been to extend the SuperDARN coverage in the southern hemispheric, polar cap and auroral regions. Figure 1 shows the fields of view of the SuperDARN radars in the southern hemisphere. The field of view of the Zhongshan radar is depicted as a red fan with a radar boresite of 72.5°. The geomagnetic latitudes of coverage of the Zhongshan radar extend from ~60 MLAT to ~82 MLAT, including the cusp region, the auroral oval, and the polar cap region. The spatial coverage of Beam 15 includes part of the polar cap region in most MLTs.

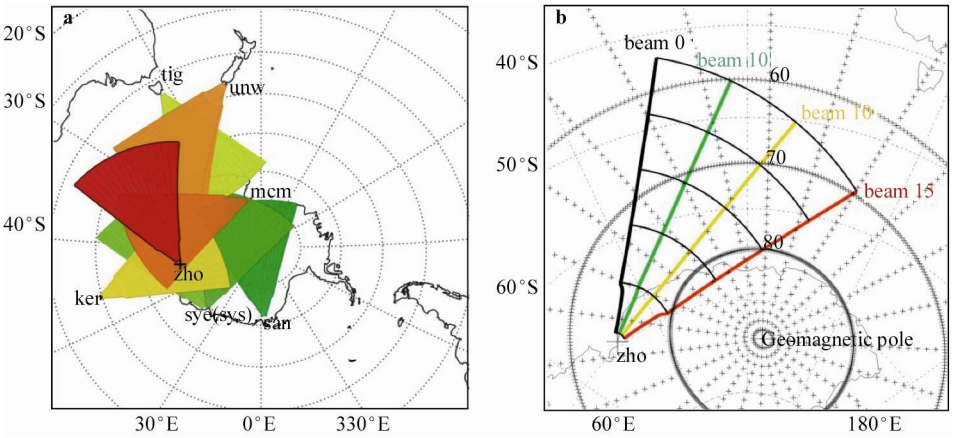

Figure 1 **a**, The fields of view of the SuperDARN radars in the Southern Hemisphere. The field of view of Zhongshan HF radar (code name zho) is illustrated by the red fan. **b**, The field of view of Zhongshan radar. Beams 0, 5, 10, and 15 are illustrated with different colours.

A large number of previous observations have concentrated on the characteristics of ionospheric echoes, either in the F region[4,8-12] or the E region[1,13-16], by using VHF, UHF and HF radar. In contrast to UHF and VHF radio waves, high frequency (HF) radio waves are very susceptible to refractive effects[17]. The orthogonality condition can be achieved between the wave vector and the Earth's magnetic field for the SuperDARN HF radars by the refraction of radio waves in the ionosphere. Hanuise et al.[18] presented the statistical characteristics of the E region echoes by employing the SHERPA radar at high latitudes. The observed echoes are both Type I and II echoes with the exception of substantially smaller spectral widths. Similarly, both these two kinds of E region echoes were also found by Haldoupis et al.[16] using a HF radar at mid-latitudes. Different statistical characteristics of backscatter echoes can be obtained for different SuperDARN radars. Parkinson et al.[19] have analyzed statistically the distribution characteristics of echo occurrence, and average Doppler velocity and width in different geomagnetic activities using the TIGER radar data in the Southern Hemisphere. Some studies have also focused on the E region[14-15,20] or the F region[9,11,21] echoes. Carter and Makarevich[22] presented a statistical analysis of E region echoes using the data of TIGER HF radar between November 2004 and December 2006. This revealed two peaks in the morning (03–09 MLT) and evening sectors (15–21 MLT) with the latter peak having a smaller maximum and being prominent only in some monthly periods. A statistical study of the occurrence of ground and ionospheric backscatter within the fields of view of the CUTLASS HF radars during the first 20 months of operation was undertaken by Milan et al.[23]. They found that the Iceland radar can observe more near-range E region backscatter than the Finland radar owing to the more zonal beam pointing direction. There are also many work[24-25] with interests in the statistical analysis and initial studies of SuperDARN radar echoes, some of which[26-27] demonstrated the distribution difference of backscatter echoes in different radar frequency bands.

This paper describes the basic characteristics of the SuperDARN Zhongshan radar, reporting the diurnal and seasonal variations, the geomagnetic activity and the frequency dependence of ionospheric echoes observed by the Zhongshan radar in its first two years' operation, during the sunspot rising interval from April 2010 to January 2012.

2 Zhongshan radar

The Zhongshan high frequency (HF) radar located at Zhongshan Station in Antarctica has been established and in operation since April 2010, supported by the Tenth Five-Year Plan for CHINARE Capacity and the Meridian Space Weather Monitoring Project, whose main objective is to observe polar ionospheric convection. The geographic coordinate of the Zhongshan Station is 69.4°S, 76.4°E, the Corrected Geo-Magnetic (CGM) coordinate is 74.5°S,

96.01°E, and the invariant magnetic latitude is ~75°S, L = 13.9, MLT≈UT+2 h, LT≈UT+5 h. During the condition of quiet geomagnetic and solar activity, Zhongshan Station is in the cusp region near magnetic noon, in the polar cap region at night, and in and out of auroral oval twice every day (under the auroral oval during 04–08 UT and 12–15 UT). Zhongshan Station has become one of the most important stations for probing and studying the variation of the space environment conditions[28-29].

Zhongshan HF radar commenced operation as soon as the radar was built and is one of the SuperDARN members. SuperDARN has been established for over 20 years. It began with the Goose Bay radar[7] and has been successful in addressing a wide range of scientific questions concerning processes in the magnetosphere, ionosphere, thermosphere, and mesosphere, as well as questions relating to general plasma physics[30-31]. As with the other SuperDARN radars, the spectral analysis of ACFs is made for Zhongshan HF radar echoes backscattered by ionospheric irregularities, and then the echo power, the line-of-sight Doppler velocity, and the Doppler power spectrum of the irregularities are estimated.

Figure 2 Zhongshan radar antenna array.

The design of the Zhongshan HF radar is similar to that of other SuperDARN radars. It comprises a main array of 16 horizontally polarized log-periodic antennae, each separated by ~15 m, operating in the frequency band from 8–20 MHz with both transmit and receive capability, and an interferometer array of 4 antennae 100 m in front of the main array, which has receive capability only, as shown in Figure 2. It is a stereo HF radar with two radar channels, whose electronics was developed by Leicester University. The Zhongshan HF radar can receive HF backscatter echoes from a slant range of 180 to 3 000 km, and at heights including the ionospheric D region, E region and F region, depending on the number of gates. In common mode, also referred to as normal scan, 16 beams are sounded with a dwell time of 3 or 7 s, producing field-of-view maps of backscatter echoes with an azimuthal coverage of over 50°, every 1 or 2 min. Each full scan commences on a GPS-synchronized two-minute boundary to ensure that all the SuperDARN radars start the scan simultaneously. Typically, 75 range gates are sampled for each beam, with a pulse length of 300 μs, which corresponds to a gate length of 45 km and a lag to the first gate of 1 200 μs (180 km). In this configuration, the maximum range of the radar is approximately 3 555 km with each field of view containing 1 200 cells. Zhongshan HF radar can work in two channels independently, for example, the all-beams scan mode is operated in channel A, the scan mode of different frequencies, and different range resolutions can be operated in channel B at the same time; thus, data with different spatial and temporal resolutions can be obtained. Zhongshan HF radar can perform different scanning patterns and different range resolutions are possible, which can be changed to study certain areas within various fields of view.

3 Statistical results

The data used in the statistical calculation were taken between April 2010 and January 2012. All parameters were obtained using the standard SuperDARN FITACF algorithm[32-33]. To eliminate possible contamination from non-ionospheric scatter echoes, those echoes with low velocity (V_{los}<30 m·s^{-1}) and narrow width (Δv<35 m·s^{-1}) are identified as ground and sea scatter, which are excluded from the statistics. The ionospheric dataset is also cleaned by excluding echoes with low power (*SNR*<3 dB).

Figure 3 summarizes the variations of backscatter occurrence rate with the day of year (DOY) on different beams for the SuperDARN Zhongshan radar. The colored lines are for the 9-day moving average value of the data points for these four beams. The discontinuities from day 117 to day 124 are because of the absence of observation during this period. We found significant differences between the beams. The beam with a larger number can observe more echoes than the beam with smaller numbers. Note that for Beam 15, two maximum occurrence peaks are found near day 92 and day 275 and the occurrence on winter days is obviously larger than that on summer days. There is also a prominent low valley from day 23 to day 26 because of strong radio wave absorption arising from a magnetic storm during these days.

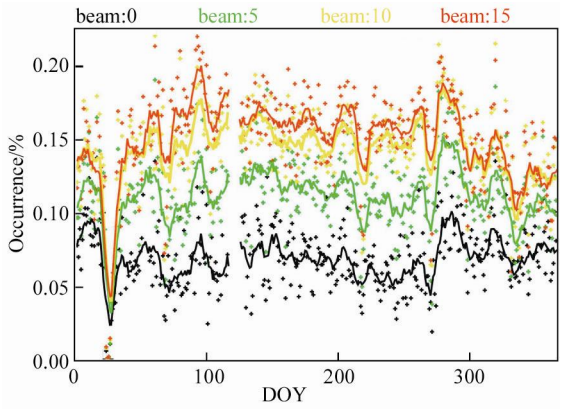

Figure 3 Variations of echo occurrence with day of year (DOY) on Beams 0, 5, 10, and 15 for the SuperDARN Zhongshan radar. The colored lines are for the 9-day moving average value of the data points.

3.1 Diurnal variations

Figure 4 shows the diurnal variations of: (a) occurrence rate, (b) average power, (c) average line-of-sight velocity and (d) spectral width of ionospheric echoes for Beams 0, 5, 10, and 15. The occurrence rate has two peaks at 04–08 UT and 16–17 UT, which vary slightly with the different beams. The value of the peak occurrence increases with beam number, and the first peak occurs earlier at smaller number beams, whereas the second peak exhibits the opposite trend. The first peak of occurrence of Beam 0 is ~10% at 04 UT, whereas Beam 15 has the peak near 08 UT with a value of ~18%. The beams with larger numbers can observe more echoes with stronger power than the beams with smaller numbers, as shown in Figures 4a and 4b. For smaller beams, the dayside valley of the occurrence is deeper than that of the nightside, which is the opposite of that for larger beams. For Beams 0 and 5, the minimum is near 13 UT, and for Beams 10 and 15, the minimum occurs at ~21 UT. Generally, the occurrence and average power have similar behavior and exhibit a double peak structure with the main peak around 04–08 UT and the second peak around 16–17 UT.

In Figure 4c, for the line-of-sight Doppler velocities, the diurnal variation is significantly different among the

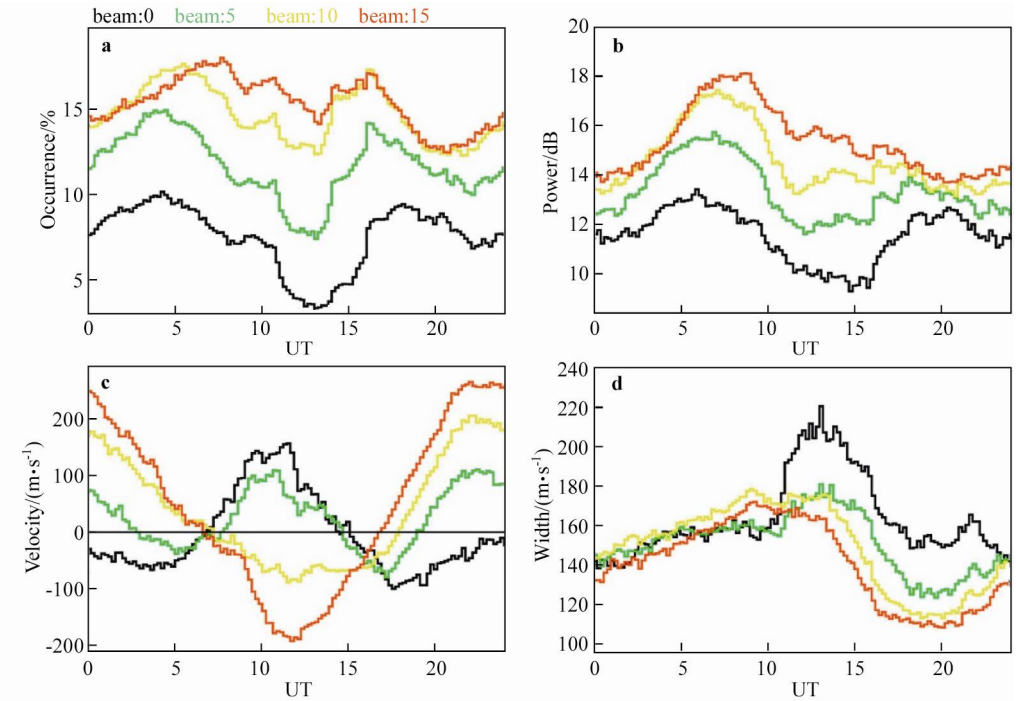

Figure 4 Diurnal variations of: **a**, occurrence; **b**, average power; **c**, average line-of-sight velocity; **d**, average width of ionospheric echoes for Beams 0, 5, 10, and 15.

beams. For Beam 0, the velocities are positive with a maximum of 160 m·s^{-1} on the dayside, which indicates that the motion is towards the radar, and mainly negative on the nightside with a maximum of −100 m·s^{-1}. The variations of Beam 15 have almost the opposite trend to that of Beam 0; the maximum of the velocities is ~260 m·s^{-1} around 22 UT for Beam 15.

In Figure 4d, the spectral widths on the dayside are often higher than those on the nightside. At 00 UT, the average widths are 130–140 m·s^{-1} and increase gradually with UT, peaking around 13 UT, and then starting to decrease steeply. The minimum appears at ~20 UT. The difference of spectral width among the different beams is not obvious from 00 UT to 11 UT. From 11 UT, the ionospheric echoes observed on Beam 0 have much larger spectral widths than on the other three beams. The maximum spectral width on Beam 0 is about 220 m·s^{-1}, whereas it is about 170 m·s^{-1} for the other beams. This might be because the echoes at near ranges of less than 30 gates on Beam 0 have more opportunities in the cusp region than the other beams, as shown in Figure 1b. In the cusp region, the echoes have greater spectral widths around noon, probably as a result of cusp particle precipitations[33].

3.2 Seasonal variations

Figure 5 shows the seasonal variations of: (a) occurrence, (b) average power, (c) average line-of-sight velocity, and (d) average widths of ionospheric echoes for Beams 0, 5, 10, and 15. The velocities are divided into two parts: positive and negative. For the echo occurrence, shown in Figure 5a, the seasonal variations are more obvious for those beams with larger numbers with maxima mainly in September and April. For Beam 15, a prominent maximum occurs in March with a secondary maximum in September, and the echo occurrence in the winter months is often larger than that in the summer months. The seasonal variation of average power is similar to that of occurrence, in the way that

the average power in winter is larger than that in summer, which might be attributed to a smaller population of irregularities owing to the solar radiation in summer. For the variations of line-of-sight velocities, the values are also obviously larger in the winter months than in the summer months for both the positive and negative components.

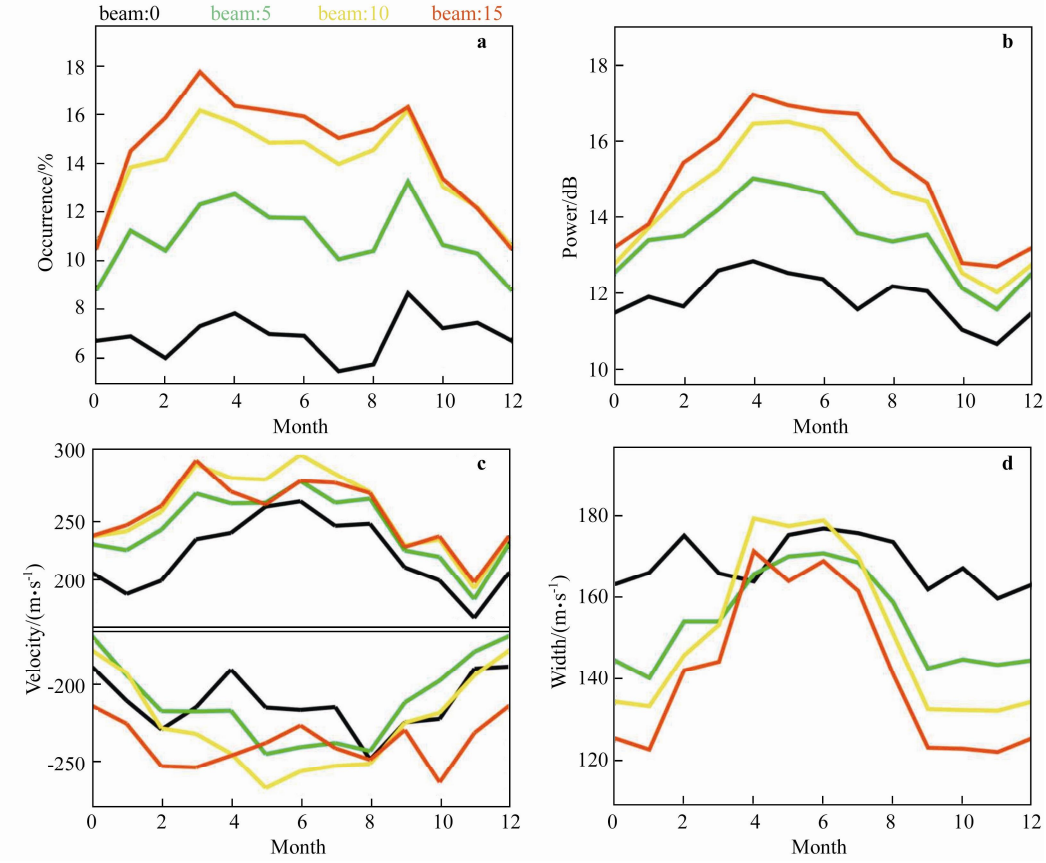

Figure 5 Seasonal variations of: **a**, occurrence; **b,** average power; **c,** average line-of-sight velocity; **d,** average width of ionospheric echoes for Beams 0, 5, 10, and 15.

In Figure 5d, the seasonal variations of spectral widths are more obvious for those beams with larger numbers. For Beam 15, the spectral widths in the winter months are significantly larger than those in the summer months with a peak value of ~170 m·s^{-1} and a broader maximum region from April to August. The spectral widths decrease to 120–130 m·s^{-1} in the summer months from September to February. For Beam 0, the seasonal variations are not obvious with the value fluctuating between 160 and 180 m·s^{-1}.

3.3 Geomagnetic activity dependence

Figure 6 shows the occurrence of ionospheric echoes at different geomagnetic activity levels. (1) For *K*p=0 (Figure 6a), the peak occurrence is between the 05–11 MLT and 79° MLAT with a value of ~45%. (2) At *K*p<2 (Figures 6a and 6b), a region with obviously low occurrence is around 22–23 MLT. This is partly due to the greater absorption in this interval associated with auroral substorms, and partly due to the polar hole that exists in this region at high latitudes[34-35]. Furthermore, the electron density of the nightside ionosphere is lower than that on the dayside and the refractive effect of the ionosphere on radio waves is weak, increasing the likelihood of the HF rays penetrating the ionosphere. (3) When *K*p increases to 2 (Figure 6c), the peak occurrence decreases obviously to about 30% between 06 and 09 MLT, expanding in MLAT of 76°–79°. When the *K*p index increases further to *K*p⩾3, the peak occurrence is at 23–03 MLT and 76° MLAT. From the geometry of Beam 15 of the Zhongshan HF radar, the echoes at lower latitudes correspond to lower gates with lower altitude, and the echo occurrence decreases obviously near 10–14 MLT on the dayside. Generally, the peak occurrence on the dayside is attributed to echoes at low levels of geomagnetic activity and decreases with the enhancement of geomagnetic activity, whereas it is the opposite on the nightside.

Figure 7 shows the average power of ionospheric echoes at different geomagnetic activity levels. From Figure 7, the presence of peak power varies for different values of the *K*p index. In quiet times with *K*p=0, large values of power are mainly in three regions. The first region is in 76°–79° MLAT from 06–13 MLT with the value greater than 20 dB. The second one is from 14–18 MLT at higher latitude with power of ~16 dB. The third one is at lower latitude 75° MLAT from 19 to 22 MLT. For *K*p=1, the region with peak power shifts to 05–15 MLT and 75°–79° MLAT, expanding

in MLT and latitude. As the geomagnetic activity increases to *K*p=2, the peak power increases from 18 dB with *K*p=1 to 21 dB with *K*p=2.

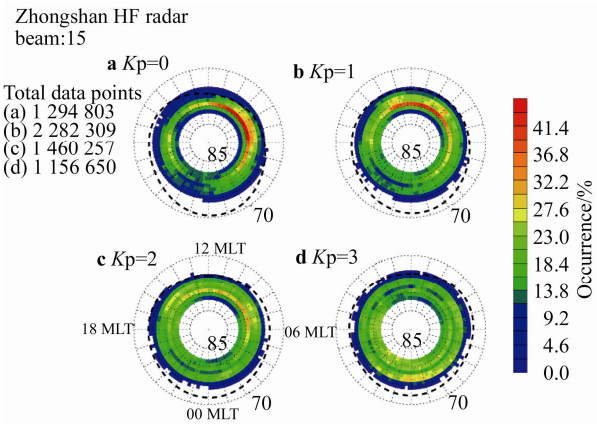

Figure 6 Occurrence of ionospheric echoes at different geomagnetic activity levels. The resolution of the grid is 1° in MLAT and 12 min in MLT. The counts of ionospheric echoes are shown at upper left corner. The thick dashed curves illustrate the poleward edge of the Feldstein auroral oval model.

Figure 8 shows the average line-of-sight Doppler velocities of ionospheric echoes at different geomagnetic activity

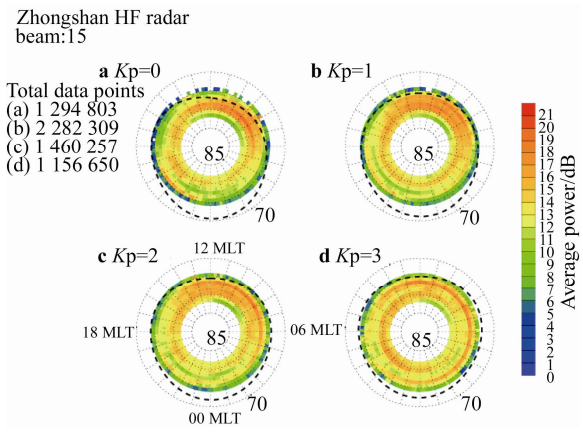

Figure 7 Average power of ionospheric echoes at different geomagnetic activity levels.

levels, the tilted dashed lines illustrate the overlay curves of MLT. The velocities increase with the enhancement of geomagnetic activity. For *K*p=0 (Figure 8a), the velocities on the dayside have a peak at about 300 m·s^{-1} and increase to more than 450 m·s^{-1} at *K*p⩾3 (Figure 8c). The same feature can also be observed on the nightside, which is consistent with the theory that ionospheric convection is enhanced with increasing geomagnetic activity.

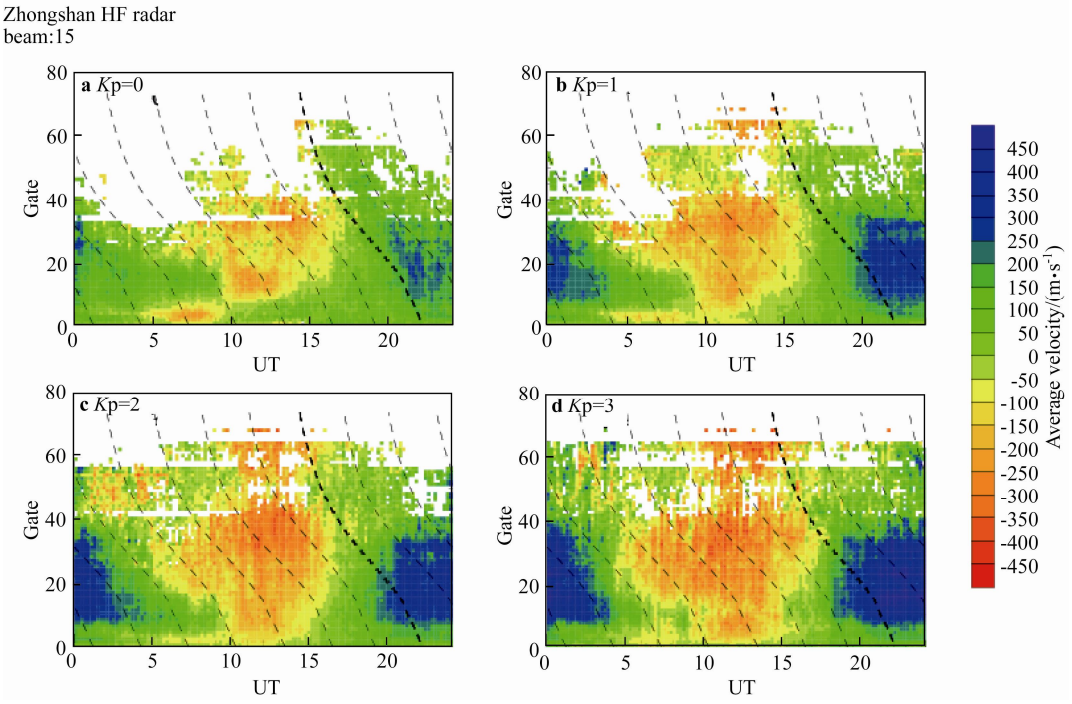

Figure 8 Average line-of-sight Doppler velocities of ionospheric echoes at different geomagnetic activity levels, the tilted dashed lines illustrate the overlay of MLT.

Figure 9 shows the average Doppler spectral widths of ionospheric echoes at different geomagnetic activity levels. As noted in Figure 9, the spectral widths on the dayside are larger than those on the nightside, which might be related to particle precipitation in the cusp region. The maximum of spectral widths decreases with the increase of geomagnetic activity. The spectral widths are quite low from duskside to nightside with a value of less than 100 m·s^{-1}, which shifts to higher latitudes when the geomagnetic activity becomes more disturbed. On the nightside, the widths tend to be lar-

ger at lower latitudes with an increase in geomagnetic activity, which might correspond to the different mechanisms of production of ionospheric echoes. Generally, the Doppler spectral width decreases with increasing geomagnetic activity, which is consistent with the results observed by Fukumoto el al.[25], using the Syowa SuperDARN radar in Antarctica.

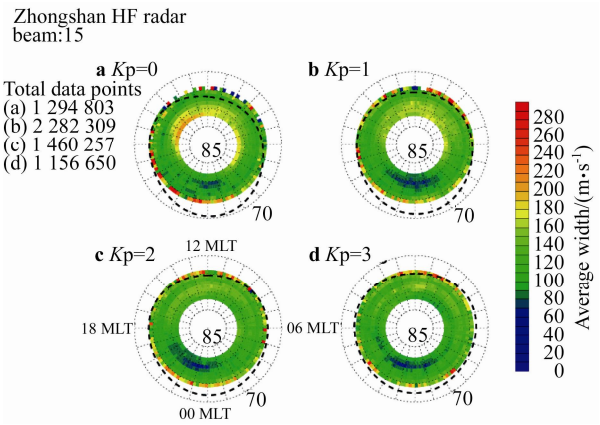

Figure 9 Average Doppler spectral widths of ionospheric echoes at different geomagnetic activity levels.

3.4 Frequency dependence

The Zhongshan HF radar was in operation with different frequencies in cycle every 2 min in channel B from 3 April to 8 October, in 2010. These frequencies are: 9, 10, 12, 13, 14, 16, and 17 MHz. The data in these frequency bands can be used to analyze the echo frequency dependence. Figure 10 shows the frequency distribution of echo occupancy rate and average power within this database. As can be observed, the average power is maximum at 9–10 MHz, and decreases slightly with increasing frequency. Regarding the echo occupancy rate, there are also more echoes observed in lower frequency band.

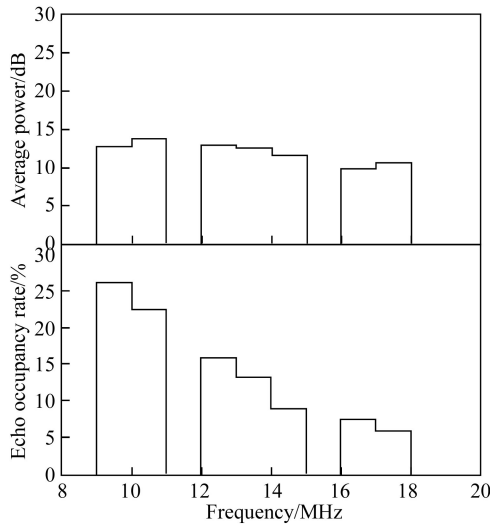

Figure 10 Frequency distribution for the database obtained in channel B of Zhongshan HF radar, showing the echo occupancy rate and average power at the seven different selected frequencies.

In summary, for Zhongshan HF radar, the echo counts decrease with frequency. Of the operating frequency bands in 2010, 9–10 MHz is the best operating frequency band; however, this might vary under different conditions of solar and geomagnetic activity.

Figure 11 presents the color-coded relative echo counts as a function of range and power for each frequency band with a resolution of 1 gate and 1 dB in power. From Figure 11 we know that there is a region with obvious ionospheric echoes less than 20 gate and 30 dB, and that the echo counts are more abundant in the low frequency bands. When the operating frequencies are 9 and 10 MHz, the echo power is mainly between 0–30 gate and 0–30 dB in power, and this region becomes narrower in range and power with increasing frequency, which is diminished to be less than 20 gate in range and less than 20 dB in power. This might be because radio waves with higher frequency are less susceptible to refractive effects in the ionosphere and tend to penetrate the ionosphere without satisfying the perpendicularity criterion, or it might be due partly to the different characteristics of the irregularities with various scale length observed by radio waves with different frequencies.

Figure 12 shows the ionospheric echo counts as a function of range and velocity for each frequency band with a resolution of 1 gate (45 km in range) and 25 $m \cdot s^{-1}$ in velocity. Figure 12 shows: (1) The velocity of most echoes is between -400 $m \cdot s^{-1}$ and 400 $m \cdot s^{-1}$; (2) The distribution of ionospheric echoes in range varies for different frequencies. In low frequency bands (9 and 10 MHz), the region with abundant echoes is less than 30 gate and decreases in range with increasing frequency; (3) When the operating frequency increases to 17 MHz, the Doppler velocity is larger from gate 5 to 20. This has to be related to the refractive properties of the ionosphere and its influence on radio wave propagation. Higher frequency waves are refracted less and the trajectories are bent more slowly along their propagation path and must propagate deeper into the ionospheric plasma, and fewer waves are backscattered by ground/sea, such that the contamination by ground scatter echoes is less for higher frequency waves, which accounts for the higher average velocity of echoes.

Figure 13 presents the echo counts as a function of range and spectral width for each frequency. The spectral width of most echoes is less than 300 $m \cdot s^{-1}$, and with increasing frequency, the width decreases. The echo spectral width is between 0 $m \cdot s^{-1}$ and 300 $m \cdot s^{-1}$ for the operating frequency of 9 MHz, while the value is between 0 $m \cdot s^{-1}$ and 200 $m \cdot s^{-1}$ for the operating frequency of 10 MHz. This is because the ionospheric irregularities that higher frequencies can observe are mainly related to high energy auroral particle precipitation and this kind of spectrum is generally considered to have narrower width.

Figure 14 shows the echo occurrence as a function of beams for different frequencies. The echo occurrence is calculated as follows: First, we calculate the echo counts $N(ut)$ of a beam from gate 0 to gate 74 and then, the ionospheric echo counts are determined according to the standard

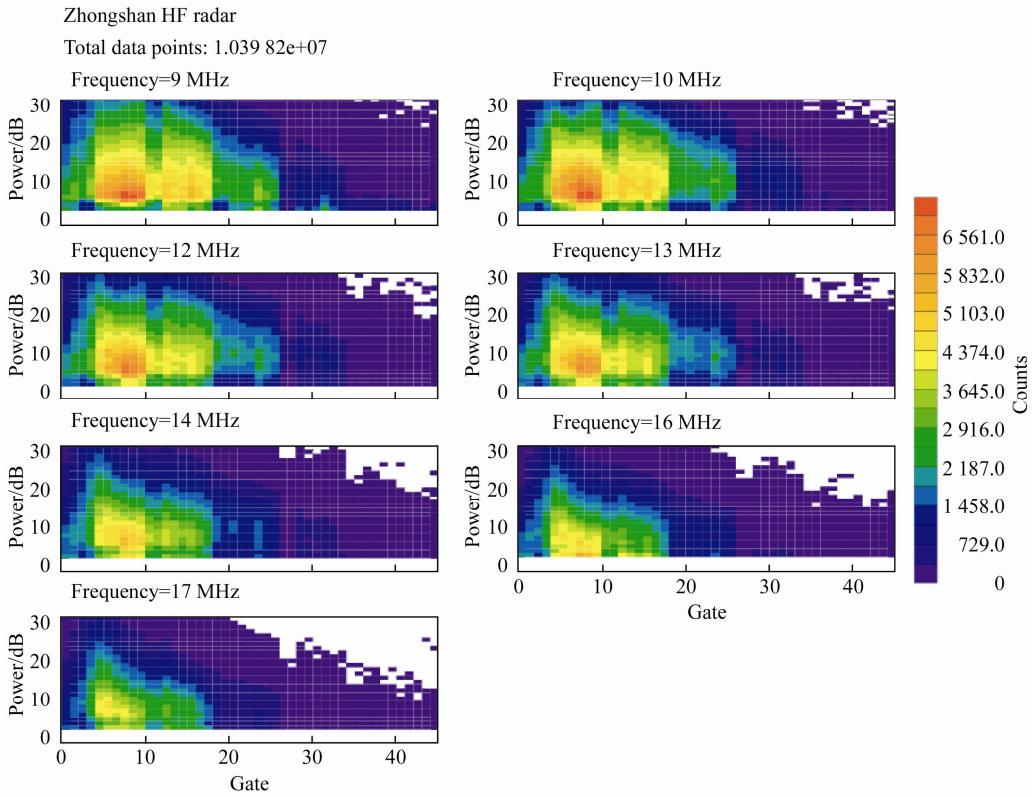

Figure 11 Distribution of ionospheric echo counts as a function of power and gate for the seven frequencies in channel B. The grid resolution is 1 in gate and 1 dB in power.

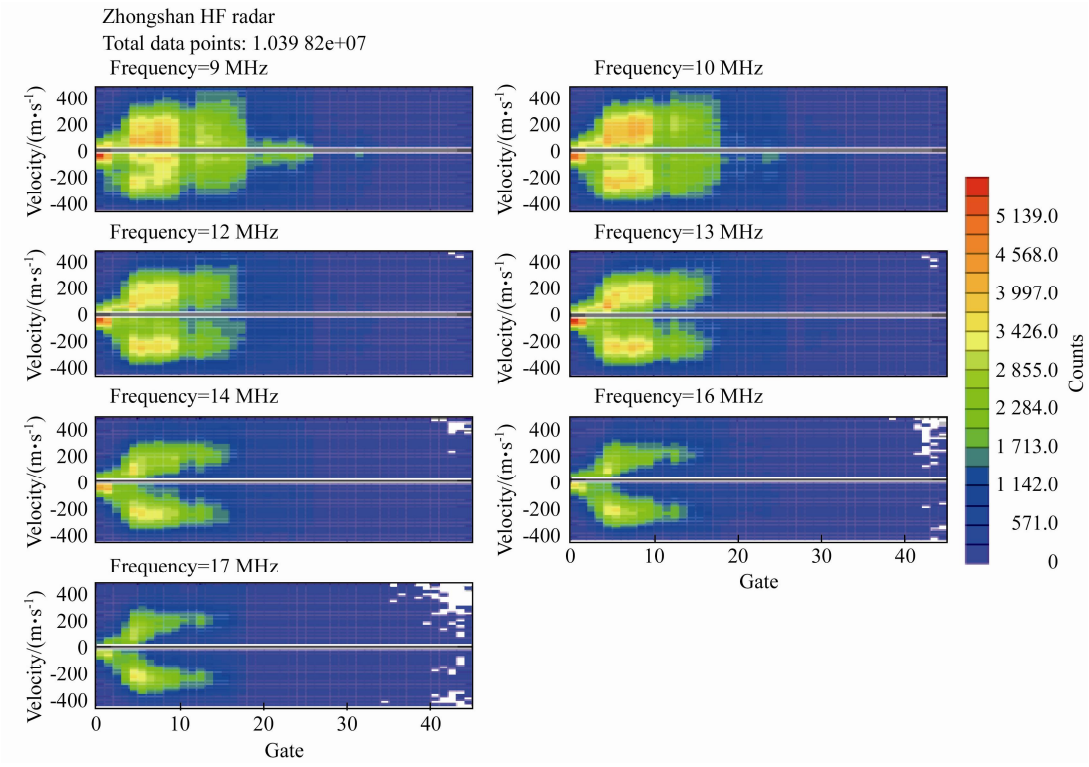

Figure 12 Distribution of ionospheric echo counts as a function of velocity and gate for the seven frequencies in channel B. The grid resolution is 1 in gate and 25 $m \cdot s^{-1}$ in velocity.

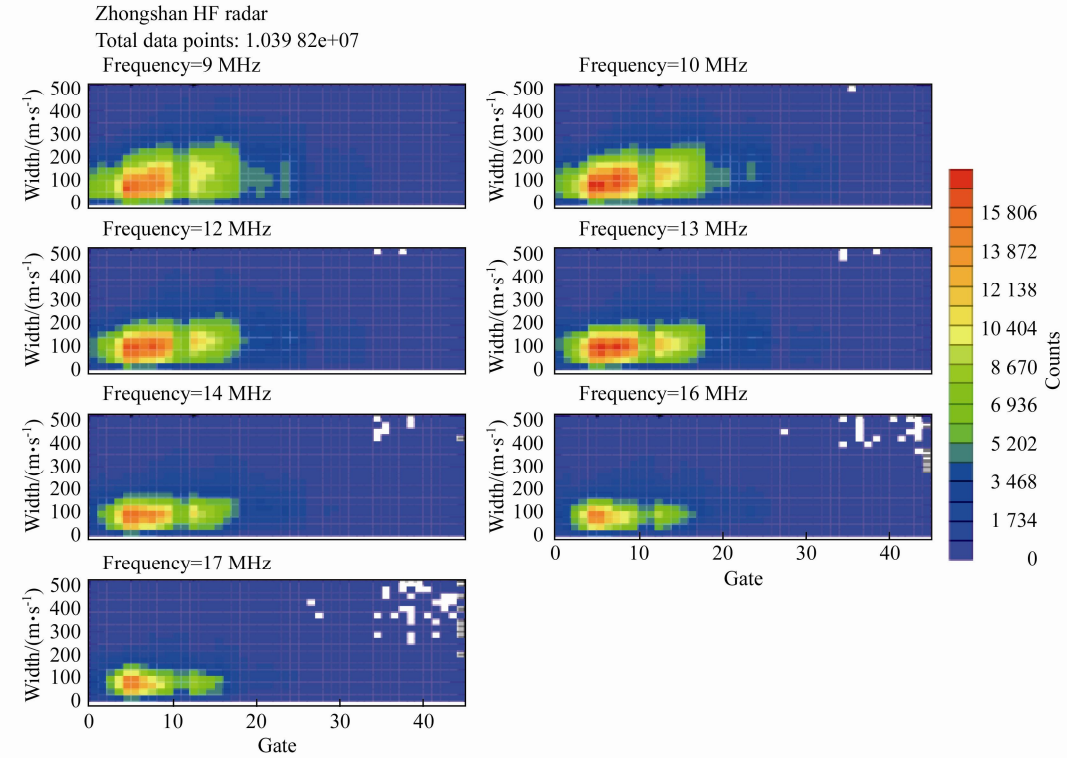

Figure 13 Distribution of ionospheric echo counts as a function of width and gate for the seven frequencies in channel B. The grid resolution is 1 in gate and 25 m·s^{-1} in width.

SuperDARN software as $M(ut)$; thus, the echo occurrence is $M(ut)/N(ut)$.

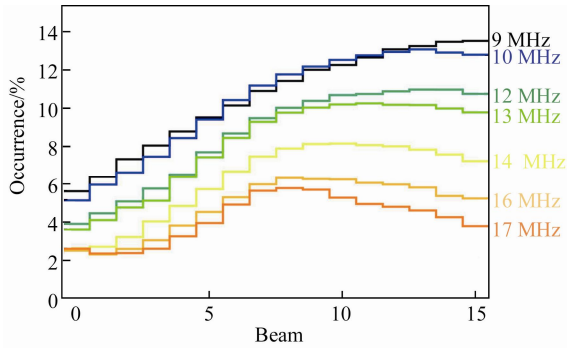

Figure 14 Occurrence histograms of ionospheric echoes on different beams for the seven frequencies.

As can be seen in Figure 14, the echo occurrence increases with the beam number for operating frequencies less than 13 MHz. For frequencies greater than 13 MHz, the echo occurrence of the center beam has the maximum value. For any frequency band, the minimum occurrence occurs on the beam with the lowest number, which might be related to the geographic and geomagnetic location of HF radar beams and the ionospheric convection modes. As the radio waves propagate through the ionosphere, they are backscattered by the decameter-scale field-aligned irregularities (FAI) when the Bragg condition is satisfied, i.e., significant backscatter is generated only if the radar wave vector lies in the plane perpendicular to the structure of FAIs[23,36]. The orthogonality condition can be achieved between the wave vector and the Earth's magnetic field for the SuperDARN radars by the refraction of HF radar waves in the ionosphere.

For the Zhongshan HF radar, the beams with small number (0–5) tend to be aligned with the Earth's magnetic field direction, which increases the orthogonality difficulty between the radio wave vector and the Earth's magnetic field; thus, the lower occurrence of echoes.

The region where HF radar can observe the irregularities can be simulated by ray tracing[37]. In the calculation, the orthogonality condition is assumed to be satisfied when the angle between HF radar ray vector and the ambient magnetic field vector is within the range of 90°±1°. In the present study, we introduce IRI-2007 electron density profiles[38] to the ray tracing and the height profile of the plasma frequency, and the ray tracing plots are shown in Figure 15. There are two distinct regions that signify possible areas in which the radar could observe if irregularities exist. These two regions are the expected locations, in both range and height, of the E region and F region echoes, respectively.

Figure 16 shows the simulation results for 10 and 16 MHz. As can be seen, in the low frequency band (10 MHz), the beams with larger number can observe the irregularities in a larger region and a greater number of irregularities can be observed. When the frequency is increased to 16 MHz, the beams near the center can observe more irregularities, which is consistent with the observations from Figure 14.

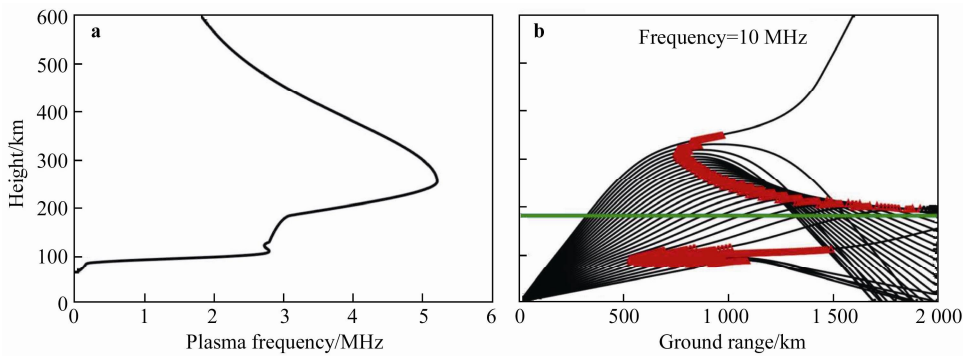

Figure 15 **a**, Vertical plasma frequency profile used in ray tracing; **b**, Simulated ray paths plot corresponding to Beam 8 of Zhongshan HF radar when the frequency is 10 MHz. The asterisks in the plot illustrate where the angle between the radio wave vector and ambient Earth's magnetic field vector is within the range of 90° ± 1°. The horizontal straight line indicates the height of 180 km. The elevation angles are from 1° to 30°.

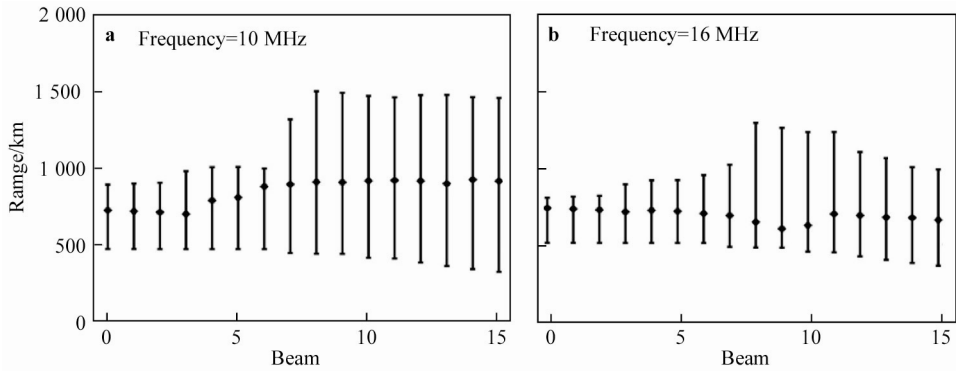

Figure 16 Possible irregularities area that Zhongshan HF radar could observe simulated by ray tracing for the frequencies of 10 and 16 MHz.

4 Discussion

Many previous works have reported on the statistical study of the characteristics of SuperDARN backscatter echoes, some of which have concentrated on the diurnal, seasonal, and geomagnetic activity variations of backscatter, and the physics of the mechanisms involved has been discussed.

Using the SuperDARN Syowa east radar data in 1995, Fukumoto et al.[25] analyzed the effect of geomagnetic activity on echo power, line-of-sight velocity and spectral widths, and summarized that the average echo power and Doppler velocity increase, and the spectral widths decrease with the enhancement of geomagnetic activity. This is consistent with the results in this study. Ruohoniemi and Greenwald[39] presented statistical results using the Goose Bay HF radar and showed that there is significant dependence on *K*p and season for echo occurrence; the highest rates of occurrence were obtained on the nightside for quiet conditions and in the afternoon for disturbed conditions and winter was the most active season. Some of their results are similar to our results, whereas others are different from those obtained in this study owing to the different locations and beam pointing of the radars. In this study, the data are mainly polar cap echoes from 2010 to 2012, which was a time of increasing solar activity and the backscatter is mainly from auroral oval and the poleward edge of the auroral oval. Carter and Makarevich[40] presented the E region diurnal variations and the effect of geomagnetic activity. It is found that the E region echo occurrence for individual radars exhibits very similar diurnal variations for low geomagnetic activity, but that the differences between radars increases with increasing activity. Ballatore et al.[41] considered the rate of scattering occurrence over a two-year period from six SuperDARN radars operating in the Northern Hemisphere and found that the HF scattering occurrence depends on the MLT, the magnetic latitude, and the local season, which was in agreement with previous observations[39,42]. Their results could be interpreted in terms of the sunlit suppression of ionospheric density gradients by more intense summer photoionization.

The statistical results in this paper demonstrate that for the echo occurrence of the SuperDARN Zhongshan radar there are two minima, which are near 13 UT and 21 UT. For Beam 0, the minimum is at 13 UT and a secondary minimum is at 21 UT, while for Beam 15, the minimum is at 21 UT and a secondary minimum is at 13 UT. The higher occurrence of echoes can be observed on Beam 15 than on Beam 0. Considering the beam pointing of Beam 0 and 15, Beam 0 is closer to the auroral oval than Beam 15. The two minimums of occurrence arise from the enhanced D region

absorption associated with isolation and particle precipitation that attenuate the propagation of HF radio waves, especially under the auroral oval near 13 UT, and the absorption event associated with substorms that are frequent at 21 UT. For Beam 15, the absorption from substorms and the little signal received from backscatter owing to the existence of the polar hole might be more prominent at 21 UT than the absorption from the D region at 13 UT, leading to the minimum near 21 UT.

Regarding the effect of geomagnetic activity on echo occurrence of Beam 15 in the grid of MLT and MLAT, the echo occurrence is at different latitudes at different values of the *K*p index. At quiet times (*K*p<2, Figures 6a and 6b), a greater number of echoes can be observed near 80° MLAT on the dayside. With an increase of geomagnetic activity to the value of *K*p≥3, a greater number of echoes are observed near 76° MLAT on the nightside. Generally, ionospheric echoes received at ranges of less than 900 km quite often originate from the E region, and sometimes from both the E and F regions[43], and this is slightly different for different radars. After considering the pointing direction of Beam 15, it is known that the echoes at these two latitude regions might come from different heights in ionosphere. At quiet times (Figures 6a and 6b), the echoes at higher latitudes might come from higher parts of the E region or F region, and at disturbed times (Figure 6d), the echoes at lower latitudes might be from lower parts of the E region. This is because particle precipitation during high geomagnetic activity leads to a large electron density in the lower ionosphere and thus, more irregularities are formed. Furthermore, the absence of the D region on the nightside ionosphere leads to little absorption of radio waves and thus, a greater number of echoes are observed at lower latitudes (lower ionosphere). This is in agreement with the finding that higher spectral widths can be observed at lower latitudes on the nightside for higher geomagnetic activity, as shown in Figure 9d.

The diurnal variations of line-of-sight velocities are very obvious. For Beam 0, the velocity is mainly positive on the dayside and negative on the nightside, which is the opposite of the variations for Beam 15. This is consistent with the fact that ionospheric convection is mainly anti-sunward in the polar cap region and sunward in low latitudes. The variations can be explained from Figure 17.

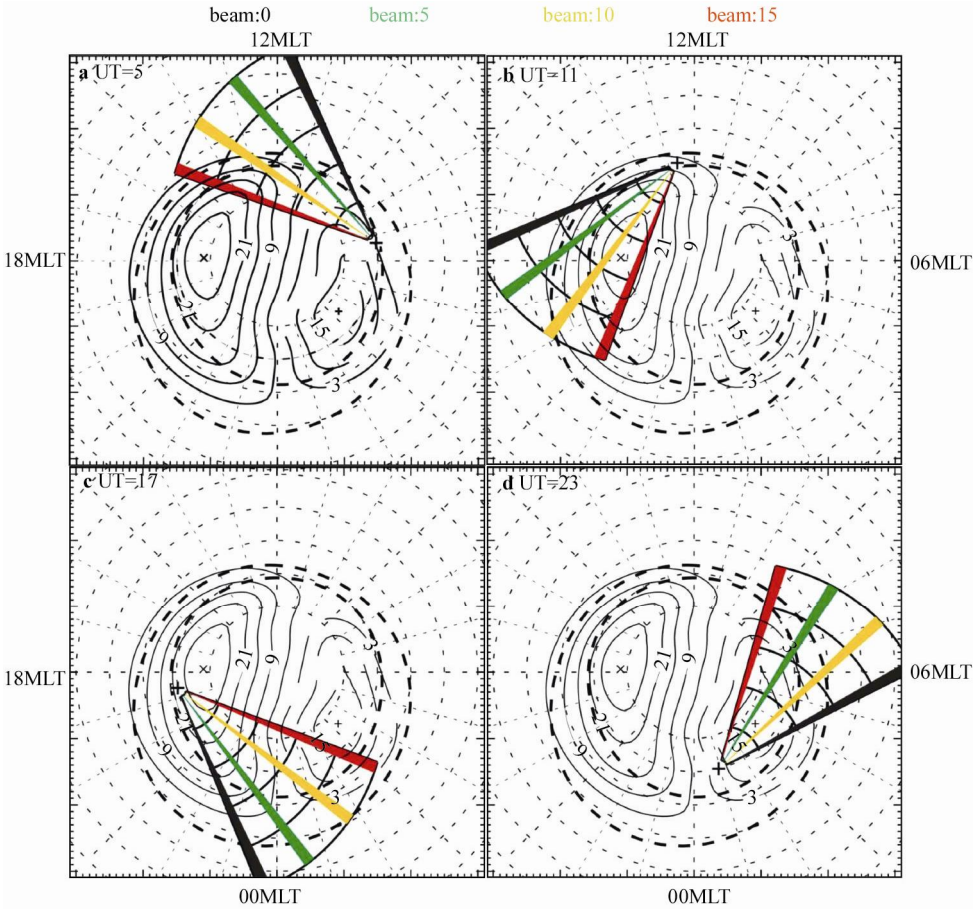

Figure 17 FOV of the Zhongshan radar at different universal times (UT). Beams 0, 5, 10, and 15 are illustrated by different colors. The dashed lines indicate the auroral oval boundary of the Feldstein model. The typical ionospheric convection twin vortex is also indicated.

At 11 UT (Figure 17b) Beam 15 is mainly pointing to the nightside and the negative velocity (away from the radar) is consistent with the anti-sunward flow in the polar cap region, and the positive velocity on Beam 0 is consistent

with the sunward flow in low latitudes. This is related to the wide azimuthal coverage of SuperDARN with values of greater than 50°. At 23 UT, shown in Figure 17d, Beam 15 is mainly pointing to the dayside and the positive velocity (towards the radar) is also consistent with the anti-sunward flow in the polar cap region, and the negative velocity on Beam 0 is also consistent with the sunward flow in low latitudes. The increase in velocities with the enhancement of geomagnetic activity is in agreement with the theory that ionospheric convection is enhanced with increasing geomagnetic activity. The velocity variations at other times are also the result of projections of the west and east components of ionospheric convection on the beam pointing direction, as shown in Figures 17a and 17c.

The spectral widths are thought to be enhanced by large-scale velocity gradients, convection turbulence, and Pc1-2 hydromagnetic wave activity[19]. Generally speaking, the spectral widths are larger in the region of open magnetic field lines on the dayside, which is also confirmed in this study. In addition, the statistics in this study also confirm that the spectral widths decrease with the enhancement of geomagnetic activity, because more high energy particles are precipitated at high geomagnetic levels, and because spectral widths from high energy particles are relatively lower than those from low energy particles. This is also consistent with the results of Fukumoto et al.[25].

We have found a marked seasonal effect on the backscatter echoes. The occurrence rate, average power, average line-of-sight velocity, and spectral widths are lower in summer than in winter. This might be related to the more intense photoionization in summer, which leads to the suppression of density gradients. This is consistent with the results of previous studies[39].

5 Conclusions

In this study, we present the statistical characteristics of ionospheric echoes based on the first two years' observations of the Zhongshan radar. These include diurnal variations, seasonal variations, geomagnetic activity, and frequency dependence. The main results are summarized as follows:

(1) Double peak structures can be observed for the diurnal variations of occurrence rate and average power, which are at 04–08 UT and 16–17 UT with a slight difference between the beams. The line-of-sight velocities for Beam 0 are mainly positive on the dayside and negative on the nightside, which is the opposite trend to that of Beam 15. These variations correspond to the anti-sunward flow in the polar cap region and the sunward flow in lower latitudes of the ionospheric convection map. The spectral widths on the dayside are often higher than those on the nightside, which is related to particle precipitation in the cusp region and Beam 0 has the most prominent peak with a value of 220 $m \cdot s^{-1}$ around 13 UT.

(2) The seasonal variations are more obvious for the beams with larger numbers. The occurrence, the average power, the line-of-sight velocity, and the spectral widths are generally larger in the winter months than those in the summer months.

(3) The difference is significant for different geomagnetic activity levels for Beam 15. Generally, the occurrence rate decreases with geomagnetic activity on the dayside and increases with it on the nightside; this arises from the solar radiation and absorption difference in MLT under the conditions of different geomagnetic activity levels. The line-of-sight velocities increase with increasing *K*p, while the Doppler spectral widths decrease with increasing geomagnetic activity.

(4) Of the frequency bands from 9 to 17 MHz used in 2010, 9–10 MHz is the best operating frequency band, but this might vary under different conditions of solar and geomagnetic activity.

(5) The difference of occurrence between beams is related to the beam pointing direction, and the different regions that the radar can observe for different frequency radio waves, arises from the area in which the orthogonality condition between the wave vector and the Earth's magnetic field is achieved.

The Zhongshan HF radar is an important component of SuperDARN, extending the coverage of the network in the polar cap region and the auroral regions in Antarctica. Further new discoveries can be expected in the future.

Acknowledgments This work was supported by the National Natural Science Foundation of China (Grant no. 41031064), the Ocean Public Welfare Scientific Research Project of China (Grant no. 201005017) and the Chinese Meridian Project, the Chinese Polar Environment Comprehensive Investigation & Assessment Programmes (Grant no. CHINARE 2012-02-03). Data were issued by the Data-sharing Platform of Polar Science (http://www.chinare.org.cn) maintained by Polar Research Institute of China and Chinese National Antarctic & Arcic Data Center.

References

1 Milan S E, Lester M. A classification of spectral populations observed in HF radar backscatter from the E region auroral electrojets. Ann Geophys, 2001, 19: 189-204.

2 Ogawa T, Nishitani N, Sato N, et al. Implications of statistics of near-range Doppler velocity observed with the Syowa East HF radar. Adv Polar Upper Atmos Res, 2001, 15: 82-102.

3 Tsunoda R T. High-Latitude F-Region Irregularities: A Review and Synthesis. Technical Report, 1 Jan. 1986—1 Jul. 1987 SRI International Corp, Menlo Park, CA, 1988.

4 Fukumoto M，Nishitani N，Ogawa T, et al. Statistical study of Doppler velocity and echo power around 75 magnetic latitude with the Syowa East HF radar. Adv Polar Upper Atmos Res, 2000, 14: 93-102.

5 Fejer B G，Kelley M C. Ionospheric irregularities. Rev Geophys, 1980, 18 (2): 401-454.

6 Greenwald R A, Baker K B, Dudeney J R, et al. DARN/SuperDARN. Space Sci Rev, 1995, 71 (1): 761-796.

7 Greenwald R A, Baker K B, Hutchins R A, et al. An Hf phased-array radar for studying small-scale structure in the high-latitude ionosphere. Radio Sci, 20(1): 63-79.

8 Koustov A V, Sofko G J, Andr D, et al. Seasonal variation of HF radar F region echo occurrence in the midnight sector. J Geophys Res, 2004, 109

(A6): A06305.
9 Hosokawa K, Iyemori T, Yukimatu A S, et al. Source of field-aligned irregularities in the subauroral F region as observed by the SuperDARN radars. J Geophys Res, 2001, 106 (A11): 24713-24731.
10 Vallieres X，Villain J P，Andre R. Characterization of frequency effect in SuperDARN spectral width distributions. Radio Sci, 2003, 38 (1): 1003-1014.
11 Villain J P, Andre R, Pinnock M, et al. A statistical study of the Doppler spectral width of high-latitude ionospheric F-region echoes recorded with SuperDARN coherent HF radars. Ann Geophys, 2002, 20: 1769-1781.
12 Hanuise C, Villain J P, Crochet M. Spectral studies of F-region irregularities in the auroral zone. Geophys Res Lett, 1981, 8: 1033-1036.
13 Makarevitch R. Formation of small-scale irregularities in the auroral E region. Canada: the University of Sakatchewan, 2003.
14 Ogawa T, Nishitani N, Sato N, et al. E region echoes observed with the Syowa HF radar under disturbed geomagnetic conditions. Adv Polar Upper Atmos Res, 2002: 84-98.
15 Makarevitch R A, Koustov A V, Sofko G J, et al. Multifrequency measurements of HF Doppler velocity in the auroral E region. J Geophys Res, 2002, 107 (A8): 1212-1223.
16 Haldoupis C, Bourdillon A, Six M, et al. Midlatitude E region coherent backscatter observed simultaneously at two HF radar frequencies. J Geophys Res, 1996, 101: 7961-7971.
17 Villain J P, Greenwald R A, Vickrey J F. HF ray tracing at high latitudes using measured meridional electron density distributions. Radio Sci, 1984, 19 (1): 359-374.
18 Hanuise C，Villain J P，Cerisier J C, et al. Statistical study of high-latitude E-region Doppler spectra obtained with the SHERPA HF radar. Ann Geophys, 1991, 9: 273-285.
19 Parkinson M L, Devlin J C, Ye H, et al. On the occurrence and motion of decametre-scale irregularities in the sub-auroral, auroral, and polar cap ionosphere. Ann Geophys, 2003, 21: 1847-1868.
20 Milan S E, Sato N, Lester M, et al. The spectral characteristics of E-region radar echoes co-located with and adjacent to visual auroral arcs. Ann Geophys, 2002, 20: 795-806.
21 Danskin D W, Koustov A V, Ogawa T, et al. On the factors controlling occurrence of F-region coherent echoes. Ann Geophys, 2002, 20: 1385-1397.
22 Carter B A, Makarevich R A. E-region decameter-scale plasma waves observed by the dual TIGER HF radars. Ann Geophys, 2009, 27: 261-278.
23 Milan S E, Yeoman T K, Lester M, et al. Initial backscatter occurrence statistics from the CUTLASS HF radars. Ann Geophys, 1997, 15: 703-718.
24 St Maurice J，Sofko G J，Wiid J, et al. First observations from the new Rankin Inlet SuperDARN radar at high northern latitudes, AGU Fall Meeting Abstracts, 2006, 1: 0354.
25 Fukumoto M, Nishitani N, Ogawa T, et al. Statistical analysis of echo power, Doppler velocity and spectral width obtained with the Syowa South HF radar. Adv Polar Upper Atmos Res, 1999, 13: 37.
26 Cowley S. The causes of convection in the Earth's magnetosphere: A review of developments during the IMS. Rev Geophys, 1982, 20 (3): 531-565.
27 Koustov A V, Igarashi K, André D, et al. Observations of 50-and 12-MHz auroral coherent echoes at the Antarctic Syowa station. J Geophys Res, 2001, 106 (A7): 12875-12,887.
28 Liu R Y, Yang H G. Progress in polar upper atmospheric physics research in China. Adv Polar Sci, 2012, 23: 55-71.
29 Hu H Q, Liu R Y, Yang H G. The auroral occurrence over Zhongshan Station, Antarctica. Chinese Journal of Polar Science, 1999, 10 (2): 101-109.
30 Chisham G, Lester M, Milan S E, et al. A decade of the Super Dual Auroral Radar Network (SuperDARN): scientific achievements, new techniques and future directions. Surv Geophys, 2007, 28 (1): 33-109.
31 Greenwald R A, Baker K B, Dudeney J R, et al. DARN/SuperDARN. Space Science Reviews, 1995, 71 (1): 761-796.
32 Ponomarenko P V, Waters C L. Spectral width of SuperDARN echoes: measurement, use and physical interpretation. Ann Geophys, 2006, 24: 115.
33 Baker K B, Dudeney J R, Greenwald R A, et al. HF radar signatures of the cusp and low-latitude boundary layer. J Geophys Res: Space Physics, 1995, 100 (A5): 7671-7695.
34 Crowley G, Carlson H C, Basu S, et al. The dynamic ionospheric polar hole. Radio Sci, 1993, 28 (3): 401-413.
35 Brinton H C, Grebowsky J M, Brace L H. The high-latitude winter F region at 300 km: Thermal plasma observations from AE-C. J Geophys Res, 1978, 83 (A10): 4767-4776.
36 Danskin D W. HF auroral backscatter from the E and F regions. Saskatoon: University of Saskatchewan Physica and Engineering Physics, 2003.
37 Jones R M, Stephenson J J. A versatile three-dimensional ray tracing computer program for radio waves in the ionosphere. US Dept. of Commerce, Office of Telecommunications, U.S. Dep. of Comm., Washington, D.C., 1975.
38 Bilitza D, Reinisch B W. International reference ionosphere 2007: Improvements and new parameters. Adv Space Res, 2008, 42 (4): 599-609.
39 Ruohoniemi J M, Greenwald R A. Rates of scattering occurrence in routine HF radar observations during solar cycle maximum. Radio Sci, 1997, 32 (3): 1051-1070.
40 Carter B A, Makarevich R A. On the diurnal variation of the E-region coherent HF echo occurrence. J Atmos Sol-Terr Physics, 2010, 72 (7-8): 570-582.
41 Ballatore P, Villain J P, Vilmer N, et al. The influence of the interplanetary medium on SuperDARN radar scattering occurrence. Ann Geophys, 2001,18(12): 1576-1583.
42 Milan S E, Yeoman T K, Lester M, et al. Initial backscatter occurrence statistics from the CUTLASS HF radars. Ann Geophys, 1997, 15(6): 703-718.
43 Koustov A V, Andre D, Turunen T, et al. Height of SuperDARN region echoes estimated from the analysis of HF radio wave propagation. Ann Geophys, 2007, 25: 1987-1984.